DETECTION OF MICROWAVE SIGNALS ASSOCIATED WITH ROCK FAILURES IN AN EARTHQUAKE FROM SATELLITE-BORNE MICROWAVE RADIOMETER DATA

Takashi Maeda

JAXA, EORC
maeda.takashi@jaxa.jp

Tadashi Takano

Nihon University
takano@ecs.cst.nihon-u.ac.jp

1. INTRODUCTION

Interferograms formed by the data of a satellite-borne synthetic aperture radar (SAR) enable us to detect slight land-surface deformations in connection with volcanic eruptions and earthquakes. However at current, since the time lag between two scenes of SAR used to form interferograms becomes longer than the recurrent period of a satellite aboard it (several tens days), it is not clear enough when land-surface deformations occur in volcanic eruptions or earthquakes.

In order to solve this problem, we have investigated another approach to detect land-surface deformations with shorter time resolution from the data of satellite-borne sensors. It was recently confirmed that microwave energy is emitted when rocks are fractured in laboratory experiments [1]. We first extrapolated the experimental results and estimated how much the power of microwave energy generated by rock failures in an earthquake is received by a satellite-borne radiometer. As a result, it was concluded that this microwave energy is detectable enough for a satellite-borne radiometer [2]. Microwave energy can penetrate the ionosphere, so it can be observed by satellite-borne sensors without ionospheric effects, but a large ambiguity exists in the underground propagation of microwaves. This conclusion was obtained under some assumptions for the underground propagation of microwaves. However, if land-surface deformations are detected by SAR, they are accompanied by rock failures. If rocks are crushed by land-surface deformations, the ambiguity in the underground propagation of microwaves is reduced, and microwave energy generated by rock failures becomes increasingly likely to be detected by a satellite-borne microwave radiometer.

Based on this, we have analyzed the data of the Advanced Microwave Scanning Radiometer for Earth Observation System (AMSR-E) aboard the satellite Aqua and attempted to detect a microwave signal generated by rock failures in association with land-surface deformations. In this situation, an earthquake occurred on May 12, 2008 in Sichuan, China, and deformation of the land surface by the earthquake was detected in the wide area around the epicenter by interferograms formed by the data of a satellite-borne SAR. Therefore, using the AMSR-E's data extracted around the epicenter during the entire observation period of six years, we verified the algorithm to evaluate microwave energy generated by rock failures in the analysis of the Sichuan earthquake.

2. ANALYSIS RESULTS

The main shock of a target earthquake occurred at 06:27:58 on May 12, 2008 (UT) in Shichuan region, China. The seismic center of the main shock was estimated to be at 31.00°N, 103.23°E with a depth of 19.0 km and magnitude of 7.9 by the National Earthquake Information Center (NEIC). Figure 1 depicts the terrain around the epicenter of the main shock and locations of aftershocks. In this figure, the diamond at the origin represents the epicenter of the main shock, and circles represent the epicenters of the aftershocks. The Longmenshan Fault runs from northeast to southwest in this figure. Deformation of the land surface by the earthquake was detected around this fault by interferograms formed by the data of the Phased-Array L-band Synthetic-Aperture Radar (PALSAR) aboard the satellite ALOS.

AMSR-E observed the $1^\circ \times 1^\circ$ area in latitude and longitude centered on the epicenter of the main shock 1345 times in descending tracks during the entire observation period of six years. We first obtained distributions of brightness temperatures of vertically and horizontally polarized signals at 18.7 GHz (T_{18V} and T_{18H}) with respect to these scenes. For these scenes, the data processing method to compensate a large sampling interval of AMSR-E [3] were applied, and T_{18V} and T_{18H} were calculated at 0.01° ($\simeq$ 1 km at 30.0°N) intervals in latitude and longitude.

Various kinds of emission, absorption and scattering by a variety of factors are reflected in T_{18V} and T_{18H}, but if we focus on a difference of T_{18V} and T_{18H} at two points (ΔT_{18V} and ΔT_{18H}) with an appropriate distance, only the difference of the fluctuation by the specific cause must be extracted in ΔT_{18V} and ΔT_{18H}. Each scene had 10201(=101 $\times$ 101) points (target

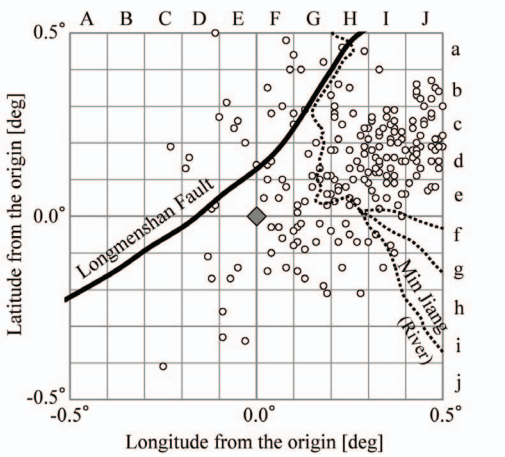

Fig. 1 Epicenters of the main and aftershocks and terrain feature around the epicenter of the main shock

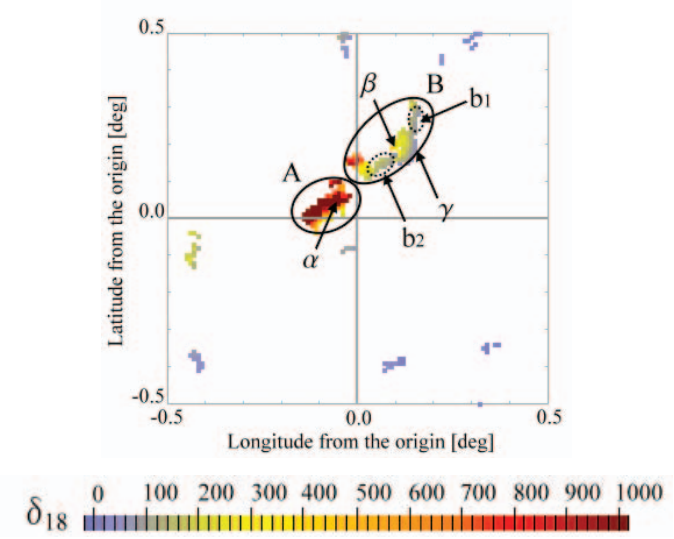

Fig. 2 Combinations of TP and RP whose S_{18} values became maximum on May 13, 2008 (one day after the main shock)

point, TP), and four points (reference point, RP) were defined for each TP (on the north, south, east, and west sides). In this analysis, distances of all combinations of TP and RP were set to 0.05°, and ΔT_{18V} and ΔT_{18H} were calculated by subtracting a brightness temperature at RP from that at TP. Thus, 40804 combinations of TP and RP were defined in the area we focused on, and time-series data of ΔT_{18V} and ΔT_{18H} during the entire observation period were obtained with respect to each combination.

However, considering microwave signals emitted in the rock crush experiments, microwaves generated by rock failures are likely to be independent of polarization. Therefore, in order to simplify the detection of a polarization-independent emission at TP, the following new value S_{18} was introduced.

$$S_{18} \equiv \sqrt{\Delta T_{18V}{}^2 + \Delta T_{18H}{}^2} \ \ (\Delta T_{18V} > 0\ ,\ \Delta T_{18H} > 0)\ \ ,\ \ 0\ \ \text{(otherwise)} \tag{1}$$

Additionally, index δ_{18} was introduced in order to extract combinations whose S_{18} values become positive only in specific observations.

$$\delta_{18} \equiv S_{18,\mathrm{MAX}}/\overline{S_{18}}\ \ (\overline{S_{18}} \neq 0)\ \ ,\ \ 0\ \ \text{(otherwise)} \tag{2}$$

where $S_{18,\mathrm{MAX}}$ ($\overline{S_{18}}$) is the largest value (the time average) of S_{18} during the entire observation period. δ_{18} becomes maximum when S_{18} becomes positive only in one observation and decreases as the number of observations in which S_{18} becomes positive increases. Therefore, as δ_{18} increases, a singularity of a temporary increase of S_{18} increases as well.

We evaluated 40804 combinations by a time variation of S_{18} instead of that of ΔT_{18V} or ΔT_{18H}. As a result, the number of combinations whose S_{18} values became maximum on May 13, 2008 (one day after the main shock), is the largest during the six-year observation period. Figure 2 depicts the distribution of the 256 combinations whose S_{18} values became the largest on May 13, 2008. According to Fig. 1, the areas indicated by circles A and B in Fig. 2 are along the Longmenshan Fault Zone.

Consequently, by the algorithm we developed, it was detected that polarization-independent microwave signals were emitted at 18.7 GHz from the land surface along the Longmenshan Fault Zone on May 13, 2008 (one day after the main shock). At least, there is little doubt that these microwave signals were the most anomalous since the observation start. Considering the current capability of the algorithm, we consider that these signals were generated by rock failures or increases of land surface temperature in aftershocks.

3. REFERENCES

[1] Maki, K., T. Takano, E. Soma, S. Yoshida and M. Nakatani, An Experimental Study of Microwave Emissions from Compression Failure of Rocks, *Journal of the Seismological Society of Japan, 58, 4*, 375 - 384, 2006.

[2] Takano, T. and T. Maeda, Experiment and Theoretical Study of Earthquake Detection Capability by Means of Microwave Passive Sensors on a Satellite, *IEEE Geoscience and Remote Sensing Letters, 6, 1*, 107 - 111, 2009.

[3] Maeda, T. and T. Takano, Discrimination of Local and Faint Changes from Satellite-borne Microwave Radiometer Data, *IEEE Trans. on Geoscience and Remote Sensing, 46, 9*, pp. 2684-2691, 2008.